# Solute effect on oxygen diffusion in α-titanium

Henry H. Wu and Dallas R. Trinkle

## Additional information on J. Appl. Phys.

# Solute effect on oxygen diffusion in α-titanium

Henry H. Wu and Dallas R. Trinkle

*Department of Materials Science and Engineering, University of Illinois, Urbana-Champaign, Illinois 61801, USA*

We calculate first-principles interaction energies between substitutional solutes and oxygen interstitials in α-titanium and predict the effect of solutes on oxygen diffusion from those interactions. Interaction between 45 solutes across the periodic table and three oxygen interstitial sites are calculated with density-functional theory. The interaction energies show distinct trends across the periodic table corresponding to both atomic radii and the period. Changes in diffusion barrier due to solutes are modeled with the kinetically resolved activation barrier approximation. Solute effects at infinite dilution are numerically calculated and show both accelerated and reduced oxygen diffusivity. © *2013 AIP Publishing LLC*. [http://dx.doi.org/10.1063/1.4808283]

## I. INTRODUCTION

Titanium alloys are limited in high temperature applications by oxidation, which makes the metal brittle, and requires costly processing steps to avoid.[1] Designing titanium alloys with high oxygen resistance has the potential to bring about cheaper light-weight alloys for aerospace[2] and medical implant[3] applications. Increasing the oxygen content in titanium forms ordered layered-oxide phases, which rely on the diffusion of oxygen into alternating basal planes to form.[4–7] These oxides are brittle and facilitate further penetration of oxygen into titanium. One could consider different possible approaches to solve this problem: designing titanium alloys to reduce the high oxygen solubility (33 at. %) in pure α-titanium; forming oxidation resistant surface coatings and films to prevent initial oxidation; engineering titanium alloys with lower innate oxygen diffusivity to slow the oxidation rate. We consider the last approach and seek to understand how various substitutional solutes impede or accelerate the diffusion of oxygen through titanium.

Oxygen occupies three interstitial sites in α-titanium, octahedral, hexahedral, and crowdion.[8] Oxygen diffusion is facilitated by heterogenous transitions between different types of interstitials. There is limited experimental data available for oxygen diffusion in Ti-rich alloys.[9–12] Computational studies on how solutes interact with and affect the diffusion of oxygen in titanium are also lacking due to how recently the new meta-stable interstitial site were discovered.

We use first-principles methods to calculate the interaction—attractive or repulsive—between oxygen interstitials and solute additions in the α-titanium matrix. We find that almost no solute from across the periodic table is able to attract and trap the oxygen in its ground-state octahedral site. These solute interaction energies are inputs for our numerical diffusion model to predict the effect solutes have on oxygen diffusivity through titanium. We find that no single solute is able to significantly reduce oxygen diffusivity through titanium while several—Na, K, Co, Y, etc.,—accelerates oxygen diffusivity. This work illustrates a systematic study of how solutes from across the periodic table affect interstitial diffusion.

## II. COMPUTATIONAL DETAILS

The first-principles calculations are performed with VASP,[13–16] a plane-wave density-functional theory (DFT) code. Ti, O, and most solute elements are treated with ultrasoft Vanderbilt type pseudopotentials,[17,18] and the generalized gradient approximation of Perdew and Wang.[19,20] Projector augmented-wave (PAW) method[21] with the PBE (Perdew-Burke-Ernzerhof) generalized gradient approximation[22] was used to treat Ge, La, Mn, and Na. The pseudopotential valence information for all solutes is listed in Appendix A. We use a single oxygen atom with one solute atom and 95 titanium atoms in a $4 \times 4 \times 3$ HCP (hexagonal-closed packed) supercell. A plane-wave cutoff of 400 eV is used for all solutes and is converged to 0.3 meV/atom. The $2 \times 2 \times 2$ $k$-point mesh with Methfessel-Paxton smearing of 0.2 eV is converged to 1 meV/atom.[23]

Fig. 1 shows the three interstitial sites oxygen occupies in α-titanium. The octahedral site is the ground-state configuration and forms a simple hexagonal lattice, the hexahedral (+1.19 eV) sites form a hexagonal close-packed lattice, and the crowdion (+1.88 eV) sites form a kagomé lattice.[24] Oxygen diffusion is governed by heterogenous transitions between all three sites with all transitions occurring at similar rates.[8] Therefore, solute interactions with all three interstitial sites are necessary in predicting changes to oxygen diffusivity.



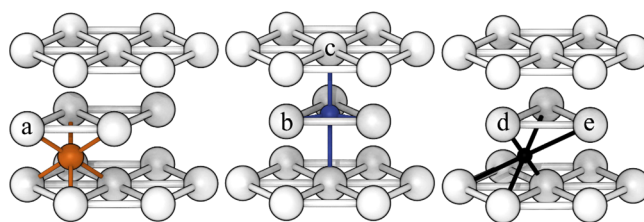FIG. 1. Position of neighboring solute for each of the three interstitial sites. The oxygen atom resides at the octahedral site (orange), hexahedral site (blue), and crowdion site (black). Solutes can occupy five substitutional positions: (a) octahedral site neighbor, (b) hexahedral site basal neighbor, (c) hexahedral site c-axis neighbor, (d) crowdion site near neighbor, and (e) crowdion site far neighbor.

Fig. 1 shows the five unique nearest neighbor positions that are possible for substitutional solutes directly surrounding the three oxygen interstitial sites. Each solute atom neighbors 6 octahedral sites, 3 hexahedral basal sites, 2 hexahedral c-axis sites, 6 crowdion near sites, and 12 crowdion far sites. The solute interaction is computed as the difference in energy between the system with oxygen neighboring the solute and away from the solute. Solutes near the oxygen are positioned according to Fig. 1; in the dissociated configuration, solutes are at least 9 Å away from the oxygen. A positive interaction energy indicates a repulsive interaction, where the oxygen does not want to be next to the solute; while a negative interaction energy indicates an attractive interaction, where the oxygen wants to be next to the solute. We also assume that the interaction between the oxygen and non-nearest neighbor solutes are zero. In Appendix B, we show that further neighbor interactions are much lower in energy than the nearest neighbor interactions and that the predicted solute effects on oxygen diffusivity do not change significantly by including additional neighbor interactions.

We link the calculated oxygen-solute interaction energies to changes in oxygen diffusion barriers with the kinetically resolved activation barrier (KRA) approximation.[25] Let $\varepsilon_i^s$ be the solute interaction energy at the interstitial site $i$, from the solute atom at the lattice site $s$. We assume additive interactions energies, thus summing over all solutes, we get $\sum_s \varepsilon_i^s$ as the total change in site energy for interstitial site $i$. The normalized reaction coordinate of the saddle point is $x_{i \to j}$ for a transition from interstitial site $i$ to interstitial site $j$. For oxygen diffusion in titanium, $x_{o \to o} = x_{o \to h} = x_{h \to o} = 1/2$, $x_{o \to c} = x_{h \to c} = 3/4$, and $x_{c \to o} = x_{c \to h} = 1/4$. The diffusion barrier from site $i$ to site $j$, $\Delta E_{i \to j}$, is approximated as

$$\Delta E_{i \to j} = x_{i \to j} \left( \sum_s \varepsilon_j^s - \sum_s \varepsilon_i^s \right) + \Delta E_{i \to j}^0, \quad (1)$$

where $\Delta E_{i \to j}^0$ is the barrier without solutes ($\Delta E_{o \to o}^0 = 3.25$ eV, $\Delta E_{o \to h}^0 = 2.04$ eV, $\Delta E_{o \to c}^0 = 2.16$ eV, $\Delta E_{h \to o}^0 = 0.85$ eV, $\Delta E_{h \to c}^0 = 0.94$ eV, $\Delta E_{c \to o}^0 = 0.28$ eV, $\Delta E_{c \to h}^0 = 0.24$ eV). Due to the number of solutes and the multitude of different combination of solute position with respect to the sites, this approximation is used instead of a large number of DFT calculations. Comparison between the KRA approximation to DFT calculated barriers show a systematic overestimation of barriers by KRA; however, this only leads to negligible changes in predictions of solute effects on oxygen diffusivity, the details of which is discussed in Appendix C.

Changes in diffusivity are calculated numerically using a similar method as described by Allnatt and Lidiard.[26] We choose a temperature of 900 K for an isolated solute in $9 \times 9 \times 9$, $10 \times 10 \times 10$, and $11 \times 11 \times 11$ supercells. These correspond to solute concentrations of $6.86 \times 10^{-4}$, $5.00 \times 10^{-4}$, and $3.76 \times 10^{-4}$, respectively. We define the infinite dilute solute effect as

$$\Delta D = \frac{1}{D(0)} \frac{dD(c)}{dc} \Bigg|_{c=0}, \quad (2)$$

where $D(c)$ is the diffusivity at solute concentration $c$, and $D(0)$ is the solute-free diffusivity. A quadratic fit of the diffusivity is done at the three concentrations above with the linear term being $\Delta D$.

## III. SOLUTE INTERACTION ENERGY

Table I and Fig. 2 show the solute interaction energies for elements across the periodic table. The octahedral site (Fig. 2(a)) with a distance of 2.09 Å between oxygen and solute gives an interaction energy that is repulsive for almost all solutes. Only Ca and Sc are weakly attractive for oxygen in the titanium lattice. Given the high affinity oxygen has for titanium, it is not surprising that almost no other element has an attractive interaction as a substitutional solute. Because the octahedral site is the ground-state interstitial site for oxygen, this means that almost no solutes act as traps for oxygen in titanium. The trend observed shows an increase in repulsion with more d-electron filling and with higher period.

The interaction energy between oxygen and solutes at the hexahedral basal site (Fig. 2(b)), with a oxygen-solute distance of 1.92 Å, form a V-shaped curve with the dip at near half d-filling. Solutes at the hexahedral basal site show a gradually increasing attractive interaction up to half d-filling, after which the interactions become significantly repulsive with higher d-filling. The 4th period exhibits a more attractive interaction than either the 5th or 6th period.

Transition metal solutes at the hexahedral c-axis site (Fig. 2(c)), with a oxygen-solute distance of 2.22 Å, do not interact strongly with oxygen. A slight attractive interaction is seen for the larger alkali and alkaline earth metals, while a slight repulsion is seen for the smaller post-transition metals. The hexahedral c-axis site is further away from the oxygen than the basal neighbor, which explains its low interaction with most solute, its attraction to larger solute, and its repulsion of smaller atoms.

The crowdion near site (Fig. 2(d)), with a oxygen-solute distance of 2.00 Å, behaves similarly to the hexahedral basal site, with a V-shaped interaction curve dipping at near half d-filling. This can be explained by the fact that both the hexahedral basal site and the crowdion near site are relatively close to the oxygen atom, and thus behave similarly. Both V-shaped curves correlates to the dip in atomic radii for the middle transition metals. Compared to the hexahedral basal site, solutes at the crowdion near site exhibit a more dramatic dip at half d-filling as well as a larger disparity between the 4th period and the other periods.

At the crowdion far site (Fig. 2(e)), with a oxygen-solute distance of 2.18 Å, most solutes destabilize the crowdion site for oxygen. Unlike the crowdion near site, where the oxygen atom is confined directly between the solute and a titanium atom, a solute at the far site pushes the oxygen closer to neighboring octahedral and hexahedral sites. Since the barrier to leave the crowdion site is only 0.24–0.28 eV, inspecting Table I shows that almost no stable far site solute has a higher interaction energy. This is because the far site solute positions displace the low symmetry crowdion interstitial. Since the crowdion far site is also further away from the oxygen than the near neighbor, we would expect it to

TABLE I. Oxygen-solute interaction energies for different oxygen and solute configurations. Interaction energies are reported in units of eV, a positive value corresponds to a repulsive interaction between the oxygen and the solute, negative value indicates an attractive interaction, while "- - - - -" indicates that the particular oxygen-solute configuration destabilizes the interstitial site. Interaction data is available publicly in Ref. 28.

The solute site order in each cell is: octahedral, hexahedral basal, hexahedral c-axis, crowdion near, crowdion far.

**Period 3**

| Site | Na (1) | Mg (2) | Al (13) | Si (14) |
|---|---|---|---|---|
| octahedral | +0.04 | +0.25 | +0.72 | +0.97 |
| hexahedral basal | +0.12 | +0.21 | +0.46 | +0.87 |
| hexahedral c-axis | −0.45 | −0.13 | +0.26 | +0.46 |
| crowdion near | +0.26 | +0.29 | +0.51 | +1.03 |
| crowdion far | −0.29 | +0.02 | −−−−− | −−−−− |

**Period 4**

| Site | K (1) | Ca (2) | Sc (3) | Ti (4) | V (5) | Cr (6) | Mn (7) | Fe (8) | Co (9) | Ni (10) | Cu (11) | Zn (12) | Ga (13) | Ge (14) |
|---|---|---|---|---|---|---|---|---|---|---|---|---|---|---|
| octahedral | +0.09 | −0.01 | −0.03 | +0.00 | +0.09 | +0.20 | +0.44 | +0.34 | +0.34 | +0.50 | +0.57 | +0.64 | +0.83 | +0.94 |
| hexahedral basal | +0.02 | +0.09 | +0.06 | +0.00 | −0.06 | −0.23 | −0.22 | −0.27 | −0.36 | +0.01 | +0.40 | +0.61 | +0.81 | +0.99 |
| hexahedral c-axis | −0.51 | −0.41 | −0.22 | +0.00 | +0.16 | +0.24 | +0.04 | −0.00 | −0.10 | +0.04 | +0.05 | +0.10 | +0.27 | +0.41 |
| crowdion near | +0.61 | +0.51 | +0.32 | +0.00 | −0.33 | −0.71 | −0.76 | −0.73 | −0.28 | +0.05 | +0.36 | +0.60 | +0.90 | +1.27 |
| crowdion far | −0.51 | −0.44 | −0.22 | +0.00 | +0.15 | +0.20 | +0.38 | −−−−− | −−−−− | −−−−− | −−−−− | −−−−− | −−−−− | −−−−− |

**Period 5**

| Site | Rb (1) | Sr (2) | Y (3) | Zr (4) | Nb (5) | Mo (6) | Tc (7) | Ru (8) | Rh (9) | Pd (10) | Ag (11) | Cd (12) | In (13) | Sn (14) |
|---|---|---|---|---|---|---|---|---|---|---|---|---|---|---|
| octahedral | +0.18 | +0.08 | +0.10 | +0.13 | +0.23 | +0.35 | +0.65 | +0.48 | +0.53 | +0.65 | +0.68 | +0.74 | +0.88 | +1.02 |
| hexahedral basal | +0.31 | +0.02 | +0.21 | +0.31 | +0.30 | +0.16 | +0.16 | −0.06 | +0.02 | +0.44 | +0.81 | +1.00 | +1.18 | +1.36 |
| hexahedral c-axis | −0.45 | −0.44 | −0.28 | −0.08 | +0.10 | +0.04 | +0.08 | −0.05 | −0.00 | +0.02 | −0.03 | +0.02 | +0.17 | +0.32 |
| crowdion near | +0.69 | +0.67 | +0.66 | +0.41 | +0.14 | −0.13 | −0.15 | +0.01 | +0.34 | +0.74 | +0.98 | +1.15 | +1.40 | +1.67 |
| crowdion far | −0.48 | −0.54 | −0.36 | −0.14 | +0.08 | +0.24 | −−−−− | −−−−− | −−−−− | −−−−− | −−−−− | −−−−− | −−−−− | −−−−− |

**Period 6**

| Site | Cs (1) | Ba (2) | La (3) | Hf (4) | Ta (5) | W (6) | Re (7) | Os (8) | Ir (9) | Pt (10) | Au (11) | Hg (12) | Tl (13) | Pb (14) |
|---|---|---|---|---|---|---|---|---|---|---|---|---|---|---|
| octahedral | +0.61 | +0.38 | +0.23 | +0.07 | +0.22 | +0.44 | +0.72 | +0.70 | +0.62 | +0.76 | +0.82 | +0.85 | +0.92 | +1.00 |
| hexahedral basal | +0.42 | +0.33 | +0.14 | +0.20 | +0.29 | +0.25 | +0.27 | +0.18 | +0.06 | +0.41 | +0.83 | +1.10 | +1.25 | +1.40 |
| hexahedral c-axis | −0.28 | −0.31 | −0.27 | −0.06 | +0.16 | +0.22 | +0.21 | +0.19 | +0.08 | +0.14 | +0.08 | +0.08 | +0.15 | +0.25 |
| crowdion near | +1.61 | +0.95 | +0.51 | +0.35 | +0.15 | −0.04 | −0.02 | +0.09 | +0.50 | +0.89 | +1.15 | +1.32 | +1.48 | +1.71 |
| crowdion far | −−−−− | −0.38 | −0.44 | −0.10 | +0.13 | +0.33 | −−−−− | −−−−− | −−−−− | −−−−− | −−−−− | −−−−− | −−−−− | −−−−− |

behave similar to the hexahedral c-axis site. For solutes which do not destabilize the interstitial, this is shown to be the case, as an attractive interaction is seen for the larger alkali and alkaline earth metals.

Most solute atoms substitute directly to the Ti HCP lattice position, however, there are four elements which do not. The mid-transition HCP metals: Os, Re, Ru, and Tc take up a lower energy, asymmetric configuration when they substitute for a Ti atom. While these elements are still metastable at the position of the replaced lattice atom, their ground-state configuration is ∼0.5 Å away in the [0001] (Ru) or [12$\bar{3}$0] (Os, Re, and Tc) directions. We have not investigated whether these off-center sites are a general result across pseudopotentials or valences. All interaction energies for these four elements are calculated with these solutes at the off-center configurations.

## IV. EFFECT OF SOLUTES ON OXYGEN DIFFUSION

Fig. 3 shows the effect of individual solutes on the diffusivity of oxygen through α-Ti at 900 K. One surprising result is the presence of solutes which accelerate the diffusivity of oxygen through titanium. Consider a simple system with only one type of interstitial site and solutes with either attractive or repulsive interactions. For attractive interactions, the diffusing species will be trapped next to the solute, while for repulsive interactions the diffusing species will be blocked by solutes. Both of these effects will inhibit the mobility of the diffusing species and one would conclude that all solutes lead to a reduction in diffusivity. The difference between the above

simple system and oxygen diffusing in α-Ti is the presence of metastable interstitial sites. Not only are there two additional metastable sites—hexahedral and crowdion—but diffusion pathways are heterogeneously linked between site types and all such transitions are active. Since most solutes repulse the ground-state octahedral site, oxygen is not trapped by any solutes. Attractive interactions at the metastable hexahedral and crowdion sites do not bring them lower than the octahedral site energy and also do not trap the oxygen. Instead, a reduction in site energy at metastable sites will reduce barriers transitioning into the site, increasing the total transition rate across the site, and lead to an increase in oxygen diffusivity.

The effect of solutes on oxygen diffusion falls into regions where the solute interaction energy switches signs. The isoelectronic solutes (Zr and Hf) show very small changes in diffusivity, this is due to their weak interaction with oxygen for all interstitial sites. To the left of this group, solutes show large variations in how much they accelerate oxygen diffusivity. The accelerating effect is due to the attractive solute interaction at the hexahedral c-axis and crowdion far sites. The magnitude of acceleration is high in this region due to the fact that 12 crowdion far sites are influenced by a single solute. Solutes with more electron filling than the Ti group show mixed diffusivity changes up to around half d-filling. The accelerating effect is now due to the attractive interaction of solutes at the hexahedral basal and crowdion near sites. The magnitude of acceleration is not as high because only 6 crowdion near sites are influenced by a single solute. Above half d-filling, all solutes slightly reduce oxygen diffusivity. In this region, solutes at all interstitial sites are repulsive or destabilizing. This makes all
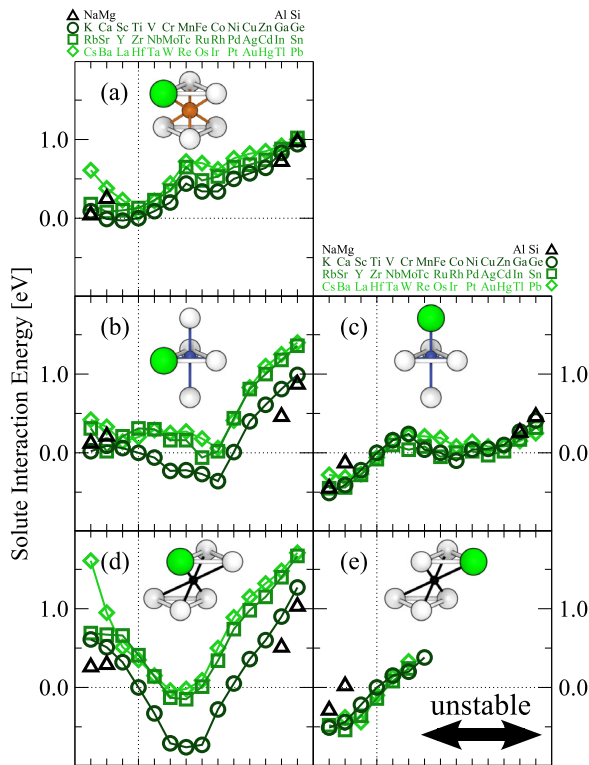
FIG. 2. Oxygen-solute interaction energies for different oxygen and solute configurations. Periodic table groups are plotted along the horizontal axis while periodic table periods are separated into different symbols. Positive energies correspond to repulsive interactions between the oxygen and the solute, while negative energies indicate an attractive interaction. Solutes positions correspond to Fig. 1: (a) octahedral site neighbor, (b) hexahedral site basal neighbor, (c) hexahedral site c-axis neighbor, (d) crowdion site near neighbor, and (e) crowdion site far neighbor.

solutes into blocking obstacles, which does not significantly inhibit oxygen diffusion until the solute concentration approaches the percolation threshold.

While Fig. 3 only shows the change in diffusivity at one particular temperature, how $\Delta D$ changes with temperature is also interesting. We define an inverse temperature derivative of the diffusivity change,

$$\Delta D' = -\left.\frac{d\Delta D}{d\beta}\right|_T, \tag{3}$$

where $\beta = (k_B T)^{-1}$.

Fig. 4 shows $\Delta D'$, which we interpret as a solute activation barrier change at a specific temperature. The values are extracted by finite difference around 900 K, specifically 850 K, 890 K, 910 K, and 950 K. The vertical axis for Fig. 4 is inverted to better show similarities to the change in diffusivity values $\Delta D$ (Fig. 3). This similarity exists because if we assume that solutes affects the diffusivity of oxygen by an Arrhenius energy barrier, $\Delta E_{act}$, that is scaled by their concentration, then

$$D(c) = D(0) \cdot \exp(-\beta \Delta E_{act} \cdot c), \tag{4}$$

where $D(0)$ is the solute-free oxygen diffusivity and $c$ is the solute concentration. Then, Eqs. (2) and (3) give

$$\Delta D = -\beta \Delta E_{act} \quad \text{and} \quad \Delta D' = \Delta E_{act}. \tag{5}$$

This shows that if the effect of the solute was purely Arrhenius, then the solute activation barrier would be linearly related to the change in diffusivity. However, this is not expected to be the case since a solute has different interactions with each interstitial site, changing the local transition barriers by varying amounts. We see the non-Arrhenius behavior in
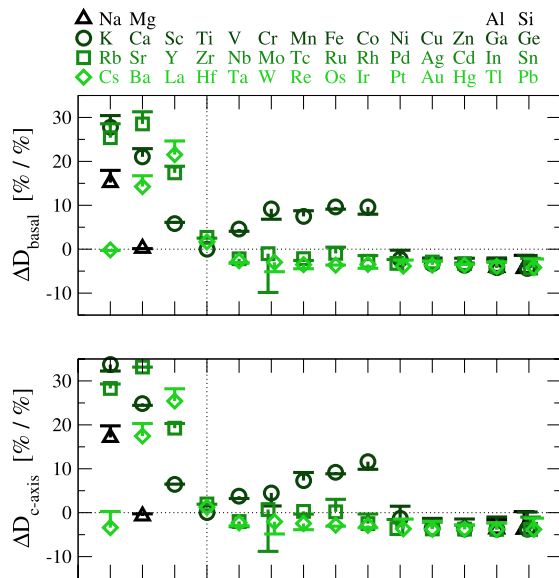


FIG. 3. Change in diffusivity of oxygen in Ti-X at 900 K. Periodic table groups are plotted along the horizontal axis while periodic table periods are separated into different symbols. The error bars indicated the effect of including second and third neighbor octahedral solute interactions, as discussed in Appendix B. Values are reported as percent change in oxygen diffusivity per atomic percent solute concentration, at the infinite dilute limit. The upper plot is for diffusion along the basal direction, while the lower plot is for diffusion along the c-axis direction.
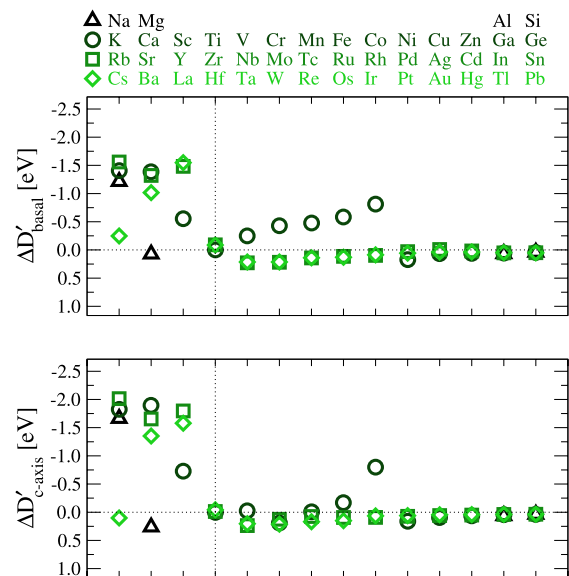


FIG. 4. Solute activation barriers to oxygen diffusion in Ti-X at 900 K. Please note that the vertical axis is inverted for direct comparison to Fig. 3, the axis limits also corresponds to those of Fig. 3 after scaling by $k_B T$ (0.0776 eV at 900 K). Periodic table groups are plotted along the horizontal axis while periodic table periods are separated into different symbols. The upper plot is for diffusion along the basal direction, while the lower plot is for diffusion along the c-axis direction.

the differences between Figs. 3 and 4, showing that $\Delta D'$ is temperature dependent.

Direct experiments looking at the effect of solutes on oxygen diffusion in titanium are scarce. Experiments also often measure the effect of solutes on oxidation, which includes the effect of oxygen dissolution as well as how the solute affects the oxide scales. For solutes such as Cr, the literature[9,10] is contradictory concerning whether Cr increase or decrease oxidation. For other solutes, such as Si,[12] results are greatly affected by the formation of titanium intermetallic particles, an effect not captured by our diffusion model. We fit the experimental results for the effect of Al up to 10 at. %,[10,11] giving –4.44 ± 3 (units of percentage change in diffusivity per atomic percent solute concentration), while the infinite dilute value from our diffusion model is −4.04 (averaged between basal and c-axis) from Fig. 3.

In addition to the magnitude of dilute limit solute effects, it is also important to consider the solubility of each solute in α-titanium.[27] More than half of the elements studied in this work have less than 1 at. % maximum solubility, though there are solutes with more significant solubilities. Zr and Hf are from the same group as titanium, and are completely miscible in α-titanium. However, they only show a minor accelerating effect on oxygen diffusivity. Al and Ga are α-stabilizers and reach a maximum solubility of up to 25 and 13 at. %, respectively. Both of these elements give a slight reduction in oxygen diffusivity. Solubility for Sn and In go up to 12 and 11 at. %, respectively, and between 5 and 10 at. % for Pb, Sc, and Cd. Out of these, only Sc shows an accelerating effect, while the others all slightly reduce oxygen diffusivity.

## V. CONCLUSION

We have used first-principles calculations to predict the effect of solutes on oxygen diffusion in α-titanium. Oxygen interstitial site energy changes in the presence of 45 solutes are calculated with DFT. The effect of solutes on oxygen diffusion barriers in titanium is modeled with the kinetically resolved activation barrier approximation from the site energy changes. A numerical diffusion framework is constructed to calculate the change in oxygen diffusivity at various solute concentrations and the infinite dilute solute effect is extracted. Trends in the oxygen diffusion change correlates with changes in sign of the solute interaction. The developed diffusion framework allows the study on how various solute distributions affect oxygen diffusion.

## APPENDIX A: PSEUDOPOTENTIAL VALENCE FOR COMPUTED SOLUTES

Table II summarizes all solutes that were considered in this work and their pseudopotential valence configurations. The Ti valence is treated as $3p^6 3d^2 4s^2$, and the O valence as $2s^2 2p^4$. All solutes used ultrasoft pseudopotentials, with the exception of Ge, La, Mn, and Na.

## APPENDIX B: EFFECT OF FURTHER SOLUTE NEIGHBOR INTERACTIONS

Fig. 5 shows calculated oxygen-solute interactions beyond the nearest neighbor position. In applying the KRA approximation to our numerical diffusion model, we have assumed that all solute interaction past the nearest neighbors in Fig. 1 are zero. This assumption reduces the number of necessary DFT calculations for each solute and simplifies the numerical model for diffusion. If the assumption does not hold, the effect would be an artificially reduced solute interaction radius with oxygen in the numerical diffusion model. However, we see in Fig. 5 that the second and third nearest neighbor solute interactions with oxygen in the octahedral site are not large in magnitude. In most cases, the interaction energy is more than a factor of 10 lower than the nearest neighbor interaction (Fig. 2(a)). This is due to the increased oxygen-solute distance of the octahedral second and third neighbor sites, 3.61 Å and 3.88 Å, respectively. These distances are much more than the five nearest neighbors we did consider (Fig. 1), which all have oxygen-solute distances of ∼2 Å. The fourth nearest neighbor for the octahedral site is 4.64 Å away from the oxygen and is expected to interact even less than the second and third neighbors.

TABLE II. Substitutional solutes and their pseudopotential valence configurations. Solutes followed by an * are treated with PAW, all others are treated with USPP (ultrasoft pseudopotential).

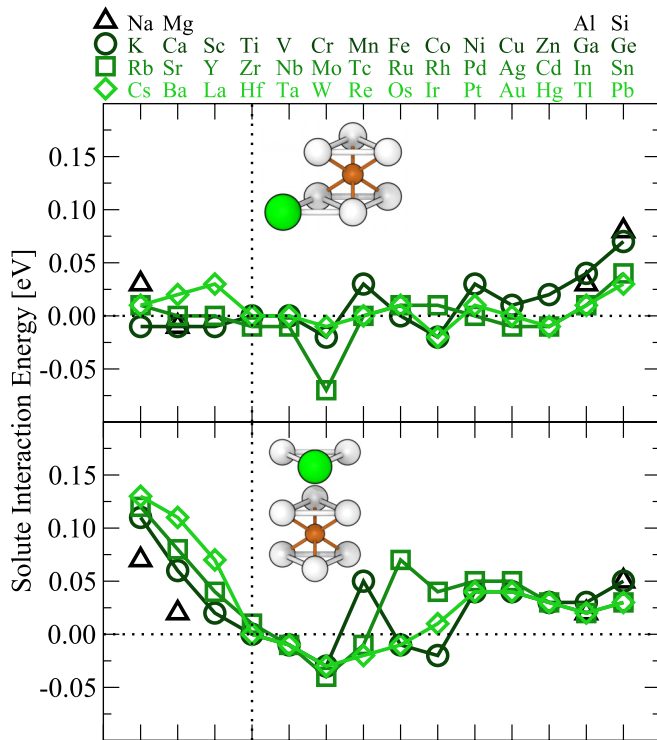| Valence configurations | | | | | | | | | |
|---|---|---|---|---|---|---|---|---|---|
| Ag | $4d^{10}5s^1$ | Al | $3s^2 3p^1$ | Au | $5d^{10}6s^1$ | Ba | $5s^2 5p^6 6s^2$ | Ca | $3p^6 4s^2$ |
| Cd | $4d^{10}5s^2$ | Co | $3d^7 4s^2$ | Cr | $3d^5 4s^1$ | Cs | $5p^6 6s^1$ | Cu | $3d^{10}4s^1$ |
| Fe | $3d^6 4s^2$ | Ga | $3d^{10}4s^2 4p^1$ | Ge* | $4s^2 4p^2$ | Hf | $5d^2 6s^2$ | Hg | $5d^{10}6s^2$ |
| In | $4d^{10}5s^2 5p^1$ | Ir | $5d^8 6s^1$ | K | $3p^6 4s^1$ | La* | $5s^2 5p^6 5d^1 6s^2$ | Mg | $2p^6 3s^2$ |
| Mn* | $3p6 3d^6 4s^1$ | Mo | $4p6 4d^5 5s^1$ | Na* | $2p^6 3s^1$ | Nb | $4p^6 4d^4 5s^1$ | Ni | $3d^8 4s^2$ |
| Os | $5d^6 6s^2$ | Pb | $5d^{10}6s^2 6p^2$ | Pd | $4d^9 5s^1$ | Pt | $5d^9 6s^1$ | Rb | $4p^6 5s^1$ |
| Re | $5d^5 6s^2$ | Rh | $4d^8 5s^1$ | Ru | $4d^7 5s^1$ | Sc | $3p^6 3d^2 4s^1$ | Si | $3s^2 3p^2$ |
| Sn | $4d^{10}5s^2 5p^2$ | Sr | $4p^6 5s^2$ | Ta | $5d^3 6s^2$ | Tc | $4d^5 5s^2$ | Tl | $5d^{10}6s^2 6p^1$ |
| V | $3p^6 3d^3 4s^2$ | W | $5d^4 6s^2$ | Y | $4p^6 4d^1 5s^2$ | Zn | $3d^{10}4s^2$ | Zr | $4p^6 4d^3 5s^1$ |

FIG. 5. Solute interaction energy beyond the first nearest neighbor of oxygen in the octahedral site. The top figure shows the second nearest neighbor configuration while the bottom is the third nearest neighbor configuration. Please note that the energy scale is a factor of 10 lower than that of Fig. 2(a). Periodic table groups are plotted along the horizontal axis while periodic table periods are separated into different symbols. Values are given in units of eV, positive values indicate repulsive interaction, while negative values indicate an attractive interaction.

The error bars in Fig. 3 show the effect of including second and third nearest neighbor interactions into our numerical diffusion model. The effect on diffusion from almost all solutes changed by less than 4 (units of percentage change in diffusivity per atomic percent solute concentration) with the addition of second and third nearest octahedral neighbor interactions. The single exception is Mo, which decreases oxygen diffusivity by approximately 10 after accounting for the second and third neighbor interactions. The reason for this decrease is due to the negative interaction between oxygen and Mo at the second and third neighbor positions, as can be seen in Fig. 5. A negative interaction means that oxygen at the octahedral ground-state is attracted to Mo solutes, and this attraction traps diffusing oxygen atoms and lead to lowered diffusivity.

## APPENDIX C: ACCURACY OF DIFFUSION MODEL APPROXIMATIONS

To calculate the effect of solutes on the diffusion of oxygen through titanium, we have used the KRA approximation to model transition barrier changes and limit solute interactions to the nearest neighbor. In this section, we will quantify the effect of the KRA approximation and show the effect of going beyond nearest neighbor interactions.

Table III compares the KRA approximation used in the diffusion model and first-principles NEB (nudged elastic band) calculations of the diffusion barriers for Al and Sc. The transitions calculated are ones where both the starting and ending

TABLE III. Comparison between transition barriers for oxygen in pure titanium, modeled using KRA from solute interactions, and direct DFT calculation with NEB. Values are given in units of eV.

|  | No solute | Al KRA | Al NEB | Sc KRA | Sc NEB |
|---|---|---|---|---|---|
| o → h | 2.04 | 1.91 | 1.81 | 2.08 | 2.05 |
| o → c | 2.16 | 2.00 | 1.88 | 2.42 | 2.37 |
| h → o | 0.85 | 0.98 | 0.87 | 0.81 | 0.78 |
| h → c | 0.94 | 0.98 | 0.89 | 1.13 | 1.10 |
| c → o | 0.28 | 0.33 | 0.15 | 0.19 | 0.13 |
| c → h | 0.24 | 0.23 | 0.09 | 0.18 | 0.14 |

configurations neighbor the same solute atom. It is at these transition saddle points that we expect the KRA approximation to be at its worst. For all transition barriers, the KRA approximation differs from the direct calculation by less than 0.18 eV. There is also a systematic overestimation of the barrier height by KRA as compared to the direct results. These errors affect the amount of time oxygen spends around the solute, however, the kinetics of sampled jumps are much less affected due to the systematic nature of the errors. When we replace those specific transitions in our diffusion model with those that were calculated directly with DFT (with all remaining barriers approximated by KRA), we obtain diffusivity results that differ by less than 0.1% when compared with the model with all KRA barriers.

[1] G. Lütjering and J. C. Williams, *Titanium*, 2nd ed., *Engineering Materials and Processes* (Springer, Berlin, 2007).
[2] R. R. Boyer, Mater. Sci. Eng., A **213**, 103 (1996).
[3] M. Long and H. J. Rack, Biomaterials **19**, 1621 (1998).
[4] S. Yamaguchi, J. Phys. Soc. Jpn. **27**, 155 (1969).
[5] T. Tsuji, J. Nucl. Mater. **247**, 63 (1997).
[6] V. B. Vykhodets, T. E. Kurennykh, and A. Y. Fishman, Defect Diffus. Forum **143–147**, 79 (1997).
[7] B. P. Burton and A. van de Walle, Calphad **39**, 97 (2012).
[8] H. H. Wu and D. R. Trinkle, Phys. Rev. Lett. **107**, 045504 (2011).
[9] I. A. Menzies and K. N. Strafford, Corros. Sci. **7**, 23 (1967).
[10] A. M. Chaze and C. Coddet, J. Mater. Sci. **22**, 1206 (1987).
[11] V. V. Vykhodets, S. M. Klotsman, T. Y. Kurennykh, and A. D. Levin, Phys. Met. Metallogr. **68**, 145 (1989).
[12] D. Vojtěch, B. Bártová, and T. Kubatík, Mater. Sci. Eng., A **361**, 50 (2003).
[13] G. Kresse and J. Hafner, Phys. Rev. B **47**, 558 (1993).
[14] G. Kresse and J. Hafner, Phys. Rev. B **49**, 14251 (1994).
[15] G. Kresse and J. Furthmüller, Comput. Mater. Sci. **6**, 15 (1996).
[16] G. Kresse and J. Furthmüller, Phys. Rev. B **54**, 11169 (1996).
[17] D. Vanderbilt, Phys. Rev. B **41**, 7892 (1990).
[18] G. Kresse and J. Hafner, J. Phys. Condens. Matter **6**, 8245 (1994).
[19] J. P. Perdew, J. A. Chevary, S. H. Vosko, K. A. Jackson, M. R. Pederson, D. J. Singh, and C. Fiolhais, Phys. Rev. B **46**, 6671 (1992).
[20] J. P. Perdew, J. A. Chevary, S. H. Vosko, K. A. Jackson, M. R. Pederson, D. J. Singh, and C. Fiolhais, Phys. Rev. B **48**, 4978 (1993).
[21] G. Kresse and D. Joubert, Phys. Rev. B **59**, 1758 (1999).
[22] J. P. Perdew, K. Burke, and M. Ernzerhof, Phys. Rev. Lett. **77**, 3865 (1996).
[23] R. G. Hennig, D. R. Trinkle, J. Bouchet, S. G. Srinivasan, R. C. Albers, and J. W. Wilkins, Nature Mater. **4**, 129 (2005).
[24] I. Syôzi, Prog. Theor. Phys. **6**, 306 (1951).
[25] A. V. der Ven, G. Ceder, M. Asta, and P. D. Tepesch, Phys. Rev. B **64**, 184307 (2001).
[26] A. R. Allnatt and A. B. Lidiard, *Atomic Transport in Solids* (Cambridge University Press, Cambridge, 1993).
[27] B. Predel, in *Landolt-Börnstein, New Series, IV/5, Phase Equilibria, Crystallographic and Thermodynamic Data of Binary Alloys*, edited by O. Madelung (Springer-Verlag, Berlin, 1991–1998), Vol. 5A–5J.
[28] Solute-oxygen interaction data available at http://hdl.handle.net/11115/125 through NIST.MatDL.org.